# Augmented reality visualisation using an image overlay system for MR-guided interventions: technical performance of spine injection procedures in human cadavers at 1.5 Tesla

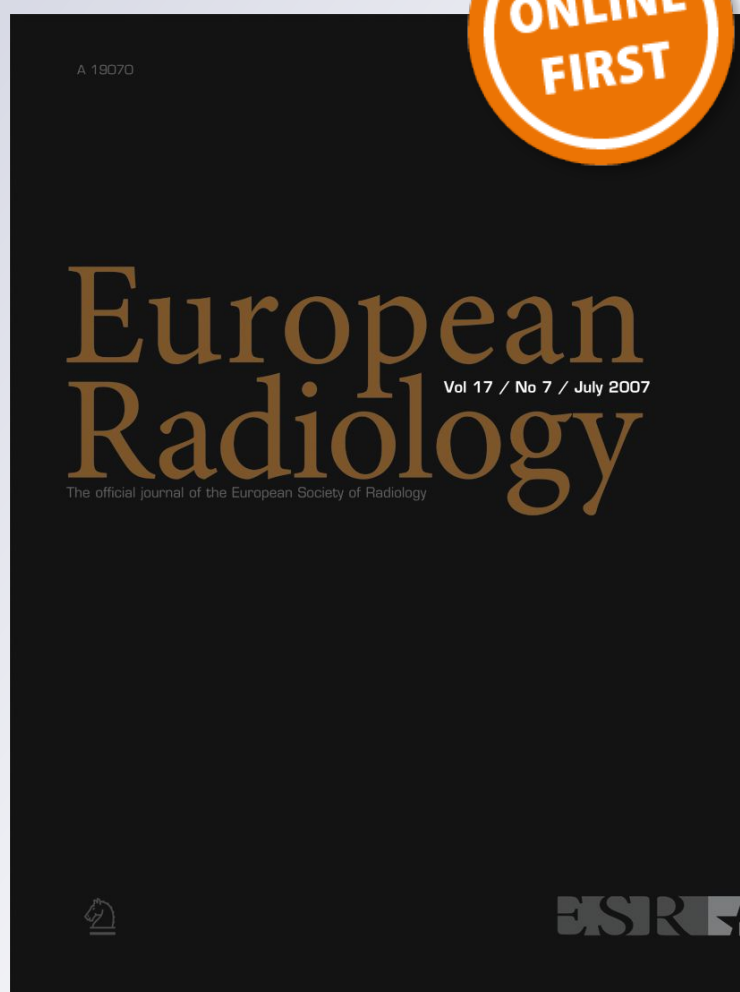**Jan Fritz, Paweena U-Thainual, Tamas Ungi, Aaron J. Flammang, Gabor Fichtinger, Iulian I. Iordachita & John A. Carrino**

ONLINE FIRST

A 19070

# European Radiology

Vol 17 / No 7 / July 2007

The official journal of the European Society of Radiology

ESR

Springer

Springer

MUSCULOSKELETAL

# Augmented reality visualisation using an image overlay system for MR-guided interventions: technical performance of spine injection procedures in human cadavers at 1.5 Tesla

Jan Fritz · Paweena U-Thainual · Tamas Ungi ·
Aaron J. Flammang · Gabor Fichtinger ·
Iulian I. Iordachita · John A. Carrino

## Abstract

*Objectives* To prospectively assess the technical performance of an augmented reality system for MR-guided spinal injection procedures.

*Methods* The augmented reality system was used with a clinical 1.5-T MRI system. A total of 187 lumbosacral spinal injection procedures (epidural injection, spinal nerve root injection, facet joint injection, medial branch block, discography) were performed in 12 human cadavers. Needle paths were planned with the Perk Station module of 3D Slicer software on high-resolution MR images. Needles were placed under augmented reality MRI navigation. MRI was used to confirm needle locations. T1-weighted fat-suppressed MRI was used to visualise the injectant. Outcome variables assessed were needle adjustment rate, inadvertent puncture of non-targeted structures, successful injection rate and procedure time.

*Results* Needle access was achieved in 176/187 (94.1 %) targets, whereas 11/187 (5.9 %) were inaccessible. Six of 11 (54.5 %) L5–S1 disks were inaccessible, because of an axial obliquity of 30˚ (27˚–34˚); 5/11 (45.5 %) facet joints were inaccessible because of osteoarthritis or fusion. All accessible targets (176/187, 94.1 %) were successfully injected, requiring 47/176 (26.7 %) needle adjustments. There were no inadvertent punctures of vulnerable structures. Median procedure time was 10.2 min (5–19 min).

*Conclusions* Image overlay navigated MR-guided spinal injections were technically accurate. Disks with an obliquity ≥27˚ may be inaccessible.

J. Fritz · J. A. Carrino
Russell H. Morgan Department of Radiology and Radiological
Science, Johns Hopkins University School of Medicine,
601 North Caroline Street,
Baltimore, MD 21287, USA

P. U-Thainual · I. I. Iordachita
Department of Mechanical Engineering and Laboratory
for Computational Sensing and Robotics,
Johns Hopkins University (JHU),
3400 N. Charles St., Hackerman 112,
Baltimore, MD 21218, USA

T. Ungi · G. Fichtinger
School of Computing, Queen's University,
557 Goodwin Hall, Queen's University,
Kingston, ON K7L 3 N6, Canada

A. J. Flammang
Siemens Corporate Research,
Center for Applied Medical Imaging,
Baltimore, MD, USA

J. A. Carrino (✉)
Musculoskeletal Division, Russell H. Morgan
Department of Radiology and Radiological Science,
Johns Hopkins University School of Medicine,
601 N Caroline St., JHOC 5165,
Baltimore, MD 21287, USA
e-mail: jcarrin2@jhmi.edu

P. U-Thainual
Department of Mechanical & Material Engineering,
Queen's University,
99 University Avenue,
Kingston, ON K7L 3 N6, Canada

Springer

*Key Points*
- *Augmented reality technology facilitates MR-guided spine injections.*
- *Patient and operator exposure to ionising radiation can be obviated.*
- *MR imaging guidance enabled the procedure without need of a dedicated interventional MRI system.*
- *Various MR-guided spine injection procedures using augmented reality are technically accurate.*
- *Augmented reality has potential to simplify the workflow of MR-guided spine injections.*

## Introduction

Spinal injection procedures, such as epidural injections, selective spinal nerve root (perineural) injections, facet joint injections, medial branch nerve blocks and discography, are commonly employed techniques in the diagnosis and treatment of back pain [1, 2]. Procedures are frequently performed under x-ray fluoroscopy and CT guidance; however, the procedure-related exposure to ionising radiation raises health concerns [1, 3–7]. Thus, over the last 2 decades, researchers have developed interventional MR imaging techniques to guide spinal injection procedures, which have successfully transitioned into clinical practice [2, 8–16]. Regardless of the advantage of the absence of ionising radiation of interventional MR imaging and achievable technical success rates similar to fluoroscopy and CT guidance, access to the patient inside the bore of the magnet is limited, which can interfere with targeting small spinal structures [16–19]. Augmented reality navigation, on the other hand, allows MR-guided procedures outside the bore with an approximate targeting error of 1.9 mm [20–23]. Thus, the purpose of this study was to prospectively assess the performance parameters (needle adjustment rate, inadvertent puncture of non-targeted structures, successful injection rate and procedural time) of this augmented reality image overlay system (IOS) for the navigation of MR-guided spinal injection procedures in human cadavers.

## Methods

### System description

An MR-compatible, two-dimensional, static axial plane augmented reality IOS was used in conjunction with a 1.5-T MRI system (MAGNETOM Espree, Siemens Healthcare, Erlangen, Germany) (Fig. 1). MR imaging guidance was provided outside the magnet by the co-registration and simultaneous visualisation of the subject and projected MR image that includes the targeted anatomical structure and planned virtual needle path [22, 24, 25]. Design, principles and components of the IOS have been detailed elsewhere [22]. The percutaneous surgery training and performance measurement module (Perk Station) of the 3D Slicer software (version 3.6, http://www.slicer.org) was used for targeting of anatomical structures, determination of the skin entry site, calculation of the virtual needle path, and display and projection of MR images [24].

### Subjects

We used 12 non-embalmed, full-torso human cadavers (7 female, 5 male; age range at death, 50–99 years; mean age at death, 75 years), including 4/12 (33 %) small (living body mass index, 16–18.5 kg/m$^2$), 4/12 (33 %) medium (18.5–25 kg/m$^2$) and 4/12 (33 %) large (25–30 kg/m$^2$) subjects [26]. Subjects were obtained and handled in accordance with our institutional policy. The frozen cadaveric subjects were allowed to thaw for 24 h to room temperature (approximately 20–22 °C) before the experiments.

### Research plan and definitions

A total of 187 lumbosacral spinal injections procedures were planned, including 7/187 (3.7 %) epidural injection, 70/187 (37.4 %) selective spinal nerve root injection, 40/187 (21.4 %) facet joint injection, 40/187 (21.5 %) medial branch nerve block and 30/187 (16 %) discography (Table 1). Each target was injected only once. The study was carried out on 18 separate days over a time period of 14 weeks. Injections were performed by one operator (J.F.) with 10 years of experience in interventional MRI and spinal injection procedures. All targets were prospectively, randomly and evenly assigned. All targets except for epidural injections were specified by lumbar level. Laterality was assigned to each target except for epidural injections and discography, which were determined individually during targeting. Procedures were executed consecutively. The operator used the dominant hand for right-sided needle paths and non-dominant hand for left-sided needle paths. Injectants consisted of gadolinium-DTPA-enhanced saline using a dilution factor of 1:250.

Epidural injections were defined as the injection of 3–5 ml of contrast medium into the lumbar epidural space through a posterior interlaminar access, selective spinal nerve root injections as the transforaminal injection of 1 ml of contrast medium to the spinal nerve, facet joint injections as the intra-articular injection of 0.5–1 ml of contrast medium into the facet joint, medial branch nerve blocks as the injection of 1 ml of contrast medium to the medial aspect of the superior surface of the transverse
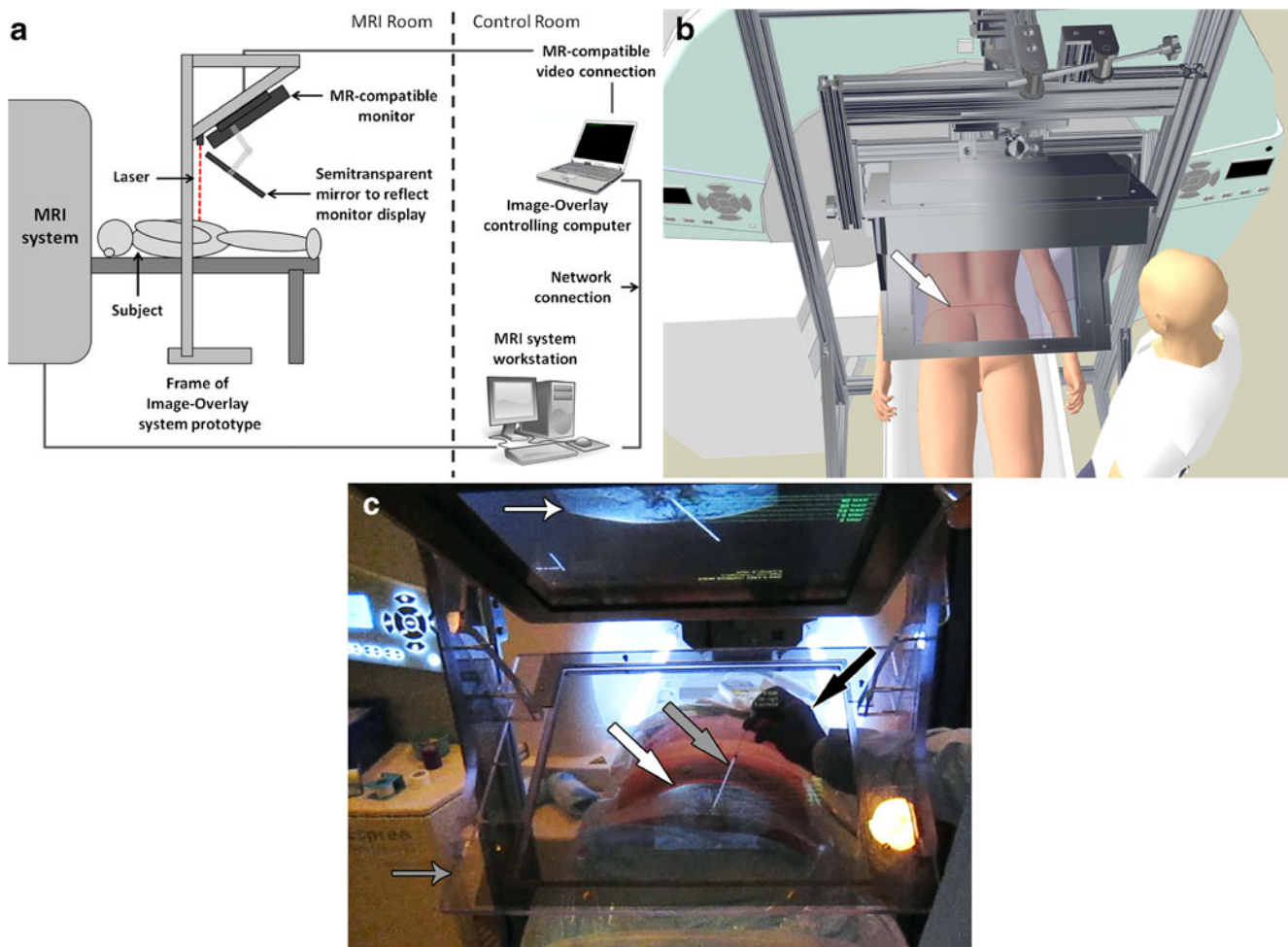
Fig. 1 a Schematic depiction of the interventional setup including the augmented reality Image-Overlay system (IOS) and a clinical 1.5-T MR imaging system. b Three-dimensional drawing of the IOS from the operator's view. The red laser line (arrow) on the subject's skin marks the target image plane in the craniocaudal direction. c Intra-procedural photograph of an MR-guided epidural injection (same as in Fig. 2) with the IOS, from the operator's view. The subject has been moved out of the magnet under the Image-Overlay, so that the target MR image (showing the target site of the epidural space) coincides with the laser line (thick white arrow). The computer fuses the target MR image with a graphical representation of the planned needle path and depth (grey arrow) and displays the composite image on the monitor display (thin white arrow). In the semi-transparent mirror (thin grey arrow) the projected image appears to be floating inside the subject in the exact location where the target MR image had been acquired. The skin entry point is indicated by the apparent intersection of the red laser line (white arrow) and the virtual needle path (grey arrow). The black arrow points to the operator's hand while inserting the needle. The composite image in the mirror does not change when the operator moves his head and it appears identical to multiple observers

process of the L1, L2, L3 and L4 lumbar vertebral body and to the notch of the ala of the sacrum (dorsal primary ramus of the L5 nerve), and discograms were defined as the injection of 1–2 ml of contrast medium into the nucleus pulposus.

Workflow

Initially, an isotropic MRI data set [three-dimensional Sampling Perfection with Application optimised Contrasts using different flip angle Evolutions (SPACE) sequence; repetition time (TR), 1,000–1,100; echo time (TE), 34; flip angle (FA), 120; number of averages (Av), 2; echo train length (ETL), 73; slice thickness (ST), 1 mm; number of slices (SL), 240; field of view (FOV), 192 × 192 mm; base resolution (BR), 192 pixels; phase resolution (PR), 100 %; bandwidth (BW), 751 Hz; acquisition time (TA), 16 min] of the lumbar spine was acquired. A flexible loop-shaped radio-frequency coil with a diameter of 19 cm (Siemens Healthcare) and the table coil elements were used for all MR image acquisitions. The MRI data set was imported into the Perk Station, and operator calibration of the IOS was performed by aligning the overlay projection with the operator's line of sight on each side of the object using the Perk Station [24].

Next, the operator selected the targets and respective skin entry points on the imported MR images using the Perk Station, which subsequently calculated and displayed needle paths and insertion depths (Fig. 2). Needle placements were

**Table 1** Procedures and vertebral levels

| Level | Epidural injection | | Selective spinal nerve root injection | | Facet joint injection | | Medial branch nerve block | | Discography | |
|---|---|---|---|---|---|---|---|---|---|---|
| | $n$ | % of total | $n$ | % of total | $n$ | % of total | $n$ | % of total | $n$ | % of total |
| L1 | - | - | 6 | 3.3 | - | - | 8 | 4.3 | - | - |
| L1-L2 | - | - | - | - | 4 | 2.2 | - | - | 6 | 3.2 |
| L2 | - | - | 8 | 4.3 | - | - | 8 | 4.3 | - | - |
| L2-L3 | - | - | - | - | 6 | 3.2 | - | - | 6 | 3.2 |
| L3 | - | - | 12 | 6.4 | - | - | 8 | 4.3 | - | - |
| L3-4 | 5 | 2.6 | - | - | 6 | 3.2 | - | - | 6 | 3.2 |
| L4 | - | - | 12 | 6.4 | - | - | 8 | 4.3 | - | - |
| L4-L5 | 2 | 1.1 | - | - | 10 | 5.3 | - | - | 6 | 3.2 |
| L5 | - | - | 12 | 6.4 | - | - | 8 | 4.3 | - | - |
| L5-S1 | - | - | - | - | 14 | 7.5 | - | - | 6 | 3.2 |
| S1 | - | - | 10 | 5.3 | - | - | - | - | - | - |
| S2 | - | - | 10 | 5.3 | - | - | - | - | - | - |
| Total | 7/187 | 3.7 | 70/187 | 37.4 | 40/187 | 21.4 | 40/187 | 21.5 | 30/187 | 16.0 |

% of total is given relative to 187 targets

performed under augmented reality MRI guidance with the subject located under the IOS (Fig. 1). For each target, the table of the MR imaging system was automatically moved to the calculated table position that resulted in appropriate location of the targeted axial image under the IOS. Augmented reality visualisation was achieved by the apparent projection of the MR image containing the target and its virtual needle path into the subject (Fig. 2). By viewing the subject through the semi-transparent mirror, a hybrid image of the actual subject and the annotated MR image were reflected to the operator (Fig. 2). The surface entry point was indicated by a laser line that was projected onto the skin surface of the subject and by the intersecting projected needle path (Fig. 1). Free-hand needle placement was performed by manoeuvring the needle along the virtual needle path. MR-compatible, 22-gauge needles (Lufkin Needle, EZ-EM, Inc., Lake Success, NY, USA) of 5- and 10-cm in length were used for facet joint injections. For all other targets, MR-compatible 20-gauge needles (MReye®, G11583, Cook Medical, Bloomington, IN, USA) of 10 or 15 cm length were used. An individually adjustable clip-on depth gauge was used to mark the planned insertion depth.

Following needle placement, turbo spin echo MR images (TR, 1,200; TE, 12; FA, 120; Av, 1; ETL, 17; ST, 3 mm; SL, 5; FOV, 256 × 224 mm; BR, 320 pixels; PR, 100 %; BW, 252 Hz; TA, 12 s) of the needle were acquired for visual assessment of the needle tip location (Fig. 2). Optional needle adjustments were performed. A maximum of four needle adjustments was permitted before a target was categorised as inaccessible.

Once the needle was in a satisfactory location, extension tubing was connected. Facet joint injections were performed outside the magnet. For all other targets, the subject was moved back into the magnet and injections were monitored by real-time MRI using a continuously acquired and displayed single-slice T1/T2*-weighted FLASH 2D MRI sequence (TR, 9.3; TE, 3.5; FA, 60; Av, 1; ST, 5 mm; FOV, 256 × 224 mm; BR, 256; PR, 56 %; BW, 180 Hz; TA, 1 s/ frame) (Fig. 2) [12]. The operator observed the injection on the display of the in-room console.

Finally, T1-weighted turbo spin echo images (TR, 500; TE, 12; FA, 120; Av, 1; ETL, 17; ST, 3 mm; SL, 7; FOV, 256 × 224 mm; BR, 320 pixels; PR, 100 %; BW, 252 Hz; TA, 32 s) with chemical fat saturation were acquired for visualisation of the injected material.

Assessment of technical performance parameters

The number of needle adjustments was assessed including needle adjustment defined as repositioning of the needle, including removal and new placement (reinsertion), change of needle trajectory (trajectory change), straight needle advancement for depth (advancement) and straight needle withdrawal for depth (withdrawal). The information was recorded during the experiments. In addition, two observers performed a retrospective consensus image analysis to assess inadvertent puncture of any non-targeted anatomical structure or vulnerable anatomical area, including the dural sac, spinal nerves and the retroperitoneum.

The rate of successful injections was assessed by two observers (JF and JAC), who independently categorised the injections into successful versus unsuccessful using a workstation. A successful injection was defined as the MRI visualisation of the injected material inside (disk,
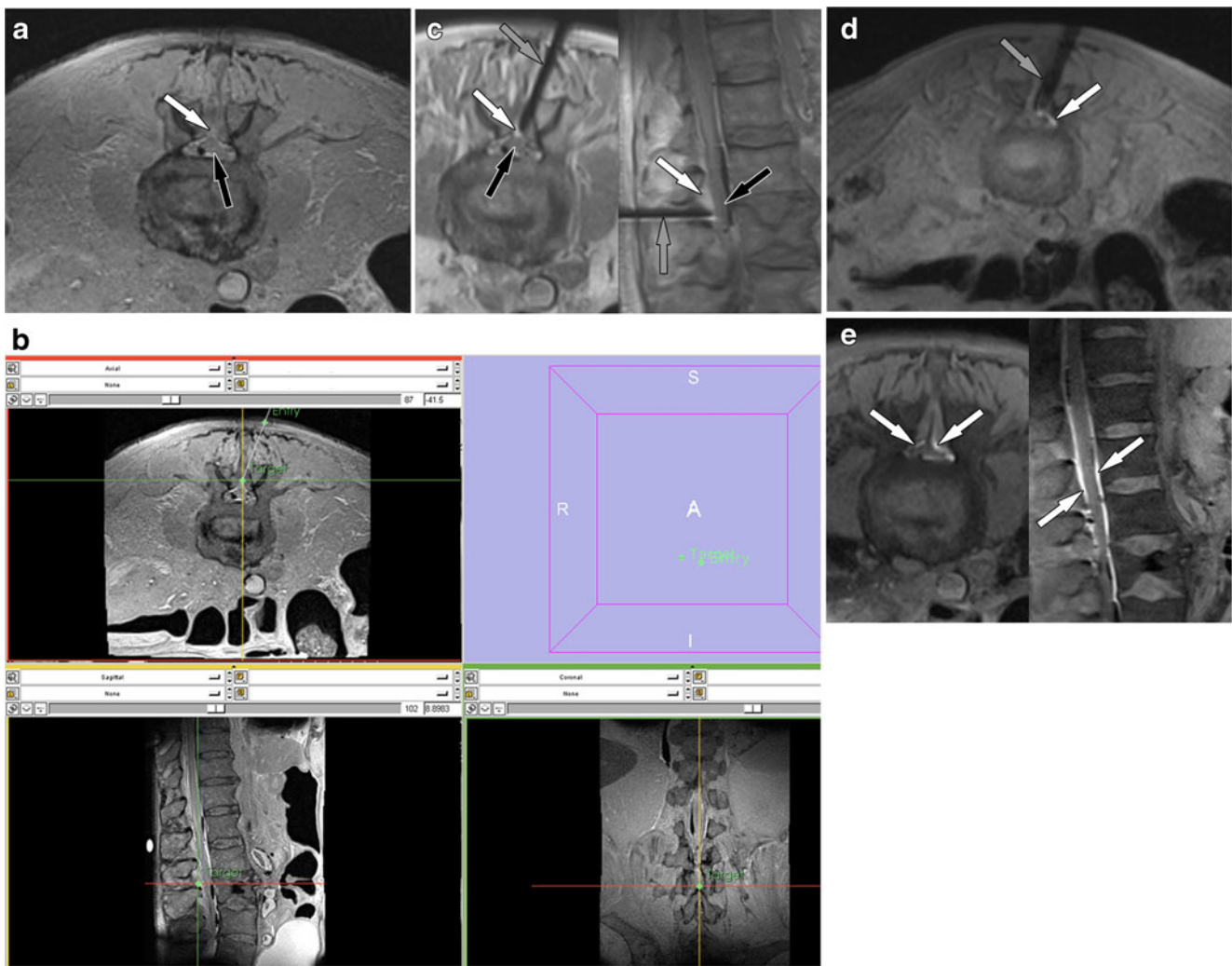
**Fig. 2** MR-guided epidural injection using image overlay navigation. **a** Axial high-resolution three-dimensional TSE MR image at the L3–L4 level demonstrates the posterior epidural fat (white arrow) situated between the medial aspects of the right and left ligamentum flavum as the target for epidural injection. The black arrow indicates the dural sac. **b** Targeting and planning of the virtual needle path using the Perk Station. **c** Axial (left) and sagittal (right) turbo spine echo MR images demonstrate the tip of the needle (grey arrows) in the posterior epidural fat pad (white arrows). The black arrow indicates the dural sac. **d** Gradient echo real-time MR image (MR fluoroscopy) for monitoring of the injection shows the needle (grey arrow) and the hyperintense injectant accumulating in the epidural space (white arrow) (see movie file). **e** Axial (left) and sagittal (right) T1-weighted MR images show the injectant in the epidural space (white arrows)

facet joint, epidural space) or around the target (median branch, spinal nerve roots). Minimal reflux along the needle track was considered acceptable for successful drug delivery. Image interpretations were performed on fat-saturated T1-weighted turbo spin echo MR images in random order, blinded to subject data, time and date. A consensus interpretation was planned for assessment differences.

A retrospective analysis of inaccessible targets was planned. The degree of obliquity and height of inaccessible disks were quantified using the measurement tool of the work station of the MR imaging system. Measurements were carried out three times by one observer. The degree of facet osteoarthritis was rated on an ordinal scale of normal, mild, moderate or severe by two observers in a consensus interpretation [27].

Assessments of time requirements including the length of time for targeting (targeting), needle placement (puncture), MR imaging control of needle position (control) and injection of the contrast agent (injection) were calculated. Procedure time was defined as the sum of targeting, puncture, control and injection times.

Statistical and quantitative assessments

Statistical analysis was performed with statistical software (JMP, version 7.01 SAS Institute Inc., Cary, NC, USA). Categorical variables were expressed as frequencies and
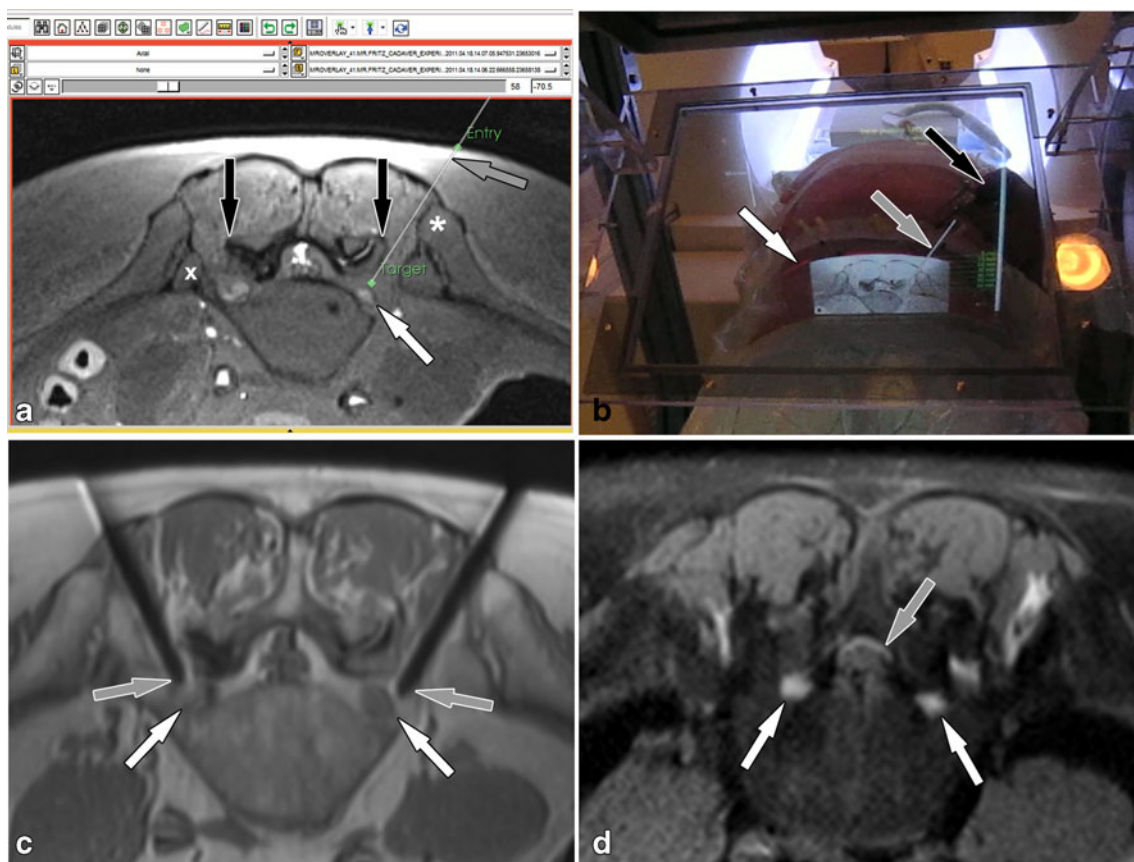
**Fig. 3** MR-guided selective injections of the left and right L5 nerve root using image overlay navigation. **a** Planning of the virtual needle path (grey arrow) to the right L5 spinal nerve (white arrow) using Perk Station. The right needle path travels between the right posterior superior iliac spine (asterisk) and the right L5–S1 facet joint (black arrow). The left needle path (not shown) travels between the left L5–S1 facet joints (black arrow) and a L5-S1 pseudoarticulation (x). **b** Intra-procedural photograph similar to the operator's view with the MR image projected onto the subject, laser line (white arrow), virtual needle path (grey arrow) and operator's hand with needle (black arrow) (see movie file Figure 3b_movie.avi). **c** Axial turbo spine echo MR image demonstrates the needle tips (grey arrows) near the L5–S1 nerve roots (white arrows). **d** Axial, T1-weighted MR image with spectral fat saturation shows the injectant in the epidural space (grey arrow) and near the exiting L5 nerves close to the neural foramina (white arrows)

proportions. Quantitative variables were expressed as the median with minimum and maximum values. A Tukey-Kramer Honestly Significant Difference test was used to compute group differences. Intra-rater variability was expressed by use of the coefficient of variation (CV) as $CV=\sigma/\mu$, where $\sigma$ is the first standard deviation and $\mu$ is the arithmetic mean. A $P$ value of less than 0.05 was considered to indicate a significant difference.

## Results

All planned procedures (187/187, 100 %) were carried out (Table 1, Figs. 2, 3, 4, 5 and 6). Needle guidance with the IOS was technically feasible in all three cadaver sizes. Needle access was achieved in 176/187 targets (94.1 %) including 7/176 (4 %) epidural injections, 70/176 (39.8 %) selective spinal nerve root injections, 35/176 (19.9 %) facet joint injections, 40/176 (22.7 %) medial branch nerve blocks and 24/176

(13.6 %) discography; 11/187 targets (5.9 %) were inaccessible, including 6/11 (54.5 %) L5–S1 disks and 5/11 (45.5 %) facet joints. Inaccessible disks showed a significantly ($P<0.001$) greater obliquity (30°, range 27-34°) when compared to the accessible L1–L5 disks (range, 2–17°) [CV=6 %; range, 0–25 %]. There was osseous fusion of one L5–S1 disk. Disk heights were not significantly different [L5–S1: 5 mm (0–9 mm), L1–L5 disks: 8-9 mm (5–14 mm), $P=0.06$-1.00, CV=6 %; range, 0–17 %]. Inaccessible facet joints showed moderate ($n=1$) and severe ($n=2$) facet osteoarthritis or osseous fusion ($n=1$). Successful injection was achieved in all accessible targets (176/187, 94.1 %), which required 47/176 (26.7 %) needle adjustments (% of total is given relative to 187 targets Table 2). There were no assessment differences. There was no evidence of inadvertent puncture of non-targeted anatomical structures such as the dural sac, spinal nerves or retroperitoneum. The median procedure time was 10.2 min (5–19 min). Procedure times for each target are given in Table 3. There was no statistically significant difference
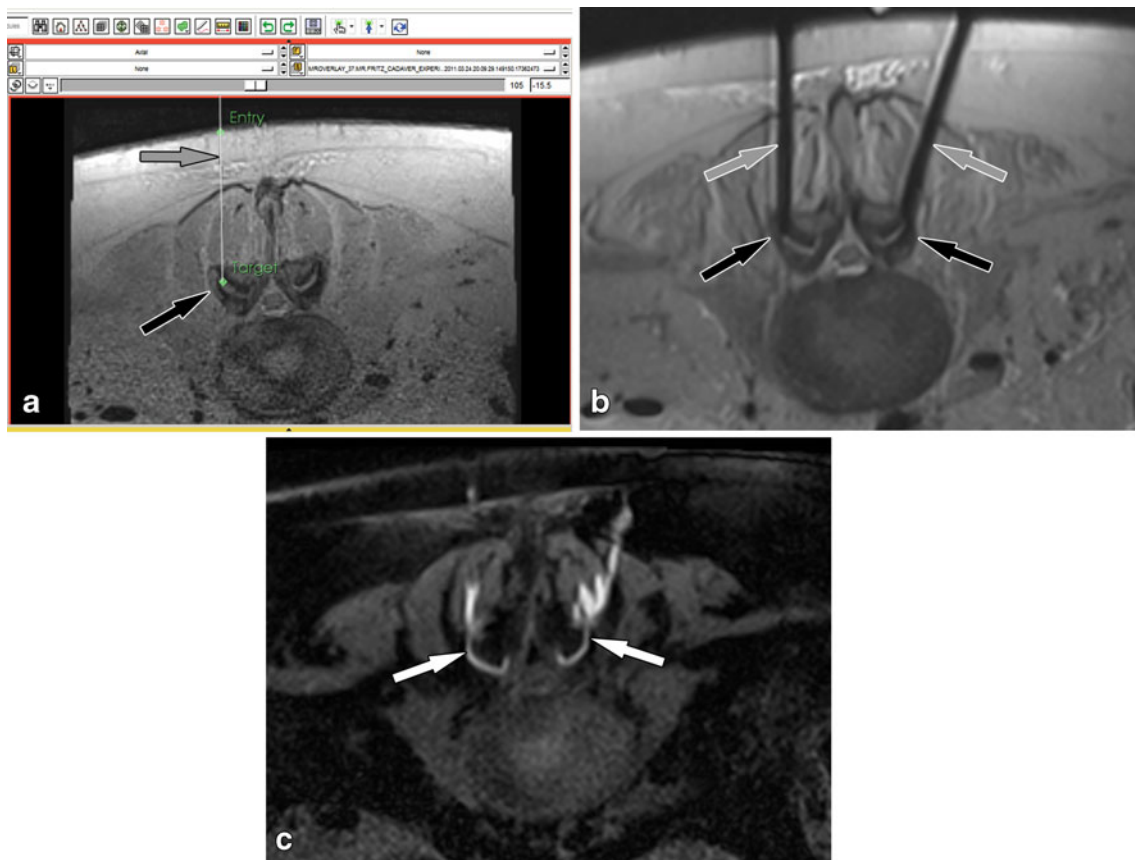
**Fig. 4** MR-guided facet joint injections using image overlay navigation. **a** Planning of the virtual needle path (grey arrow) to the left L4–L5 facet joint (black arrow) using the Perk Station. **b** Axial turbo spine echo MR image following needle placement demonstrates the tips of the needles (grey arrows) in the left and right facets joints (black arrows). **c** Axial, T1-weighted MR image with spectral fat saturation following injection shows the injectant (white arrows) in the left and right facet joints

between targets ($P$=0.86–1.00). The median targeting time was 1 min (1–3 min). The median puncture time was 2.3 min (1–5 min). The median control time was 2.5 min (1–5 min). The median injection time was 3.5 min (2–7 min).

## Discussion

Our investigation demonstrated that the technical performance of the IOS allowed for accurate lumbosacral spine injections, including epidural injections, selective spinal nerve root injections (perineural blocks), facet joint injections, medial branch nerve blocks and discograms.

Spine injections have been performed at 0.2- to 1.0-T field strength dedicated open MR imaging systems and with the more recently introduced clinical 1.5-T wide-bore MR imaging systems [10, 12, 28]. Success rates were 79.5 %–89 % for intra-articular facet joint injections [10, 12, 28], 97–100 % for selective lumbosacral nerve root injections [12, 14, 28, 29] and 97–100 % for lumbar discograms [30, 31], without the occurrence of major complications. Our data suggest that the IOS can achieve similar success rates.

Performing MR-guided spinal procedures with the IOS eliminates several limitations of interventional MR imaging, including the requirement of a dedicated interventional MRI system, limited patient access inside the magnet, and the spatial and visual separation of the interventional site and MR image [17–19, 32]. The IOS can be used with any conventional MRI system with horizontal patient orientation and an encoded table, without the need for a dedicated design.

The IOS creates an augmented reality environment by the apparent fusion of the target and the MR image [33]. This technique is different from the current practice of interventional MR imaging, which is characterised by the spatial and visual separation of the target site and MR image [9, 10, 12–15, 18, 28]. Because the targeted structure appears in the actual location of the subject and target, the IOS creates a "look and feel" ambiance without the need to mentally transfer the image information from a display onto the subject [10, 11, 14, 17–19, 21, 27].

The use of high-resolution MRI data for navigation with the IOS can improve the identification and targeting of small spinal structures. The length of time required for the acquisition of the high-resolution MRI planning volume covering one

**Fig. 5** MR-guided medial branch nerve block using image overlay navigation. **a** Planning of the virtual needle path (grey arrow) to the right L4 medial branch nerve (black arrow) using the Perk Station. **b** Axial turbo spine echo MR image following needle placement demonstrates the tips of the needles (grey arrows) at the upper edge of the transverse process (black arrows), near the anatomical location of the medial branch nerve. **c** Axial, T1-weighted MR image with spectral fat saturation following injection shows the injectant (white arrows) dispersed along the anatomical location of the medial branch nerve

spinal level ranges between 2 and 3 min. High success rates were achieved, although few facet joints were inaccessible because of degenerative changes, similar to previous reports [10, 12, 28]. Augmented reality navigation was helpful for needle access to the L5 spinal nerve in the case of an anatomical variant, such as an L5–S1 pseudo-articulation (Fig. 3), with only a narrow anatomical window for needle access.

Adverse events of spine injections are rare, but can be serious. Epidural injections through an interlaminar access carry the risk of puncture of the dural sac with subsequent intrathecal injection. The posterior epidural fat pocket situated between the medial aspects of the ligamenta flava (Fig. 2) is a relatively safe target for epidural drug delivery that was consistently visualised on the high-resolution MR image used for targeting without the occurrence of intrathecal injections.

Intravascular uptake of injected material is a recognised event during spinal injections, which occurs in 1.9–22 % of fluoroscopically guided lumbar spinal injection procedures [34–38]. Although its significance is not fully understood, it has been linked to the rare, but devastating event of spinal cord infarction after transforaminal and interlaminar lumbar epidural injections [39–44]. Although unclear, a proposed mechanism is intravascular uptake of particulate steroids, which cause embolisation injury. With use of MRI guidance, non-invasive, native MR angiography images could be obtained to assess variant anatomy such as a low origin of a dominant radiculomedullary artery branch (artery of Adamkiewicz), which may increase the risk of spinal cord infarction [42]. Empirical recommendations to detect vascular uptake before drug delivery include real-time monitoring of the injection of contrast agent [43]. As such, real-time MR monitoring of epidural injections has been used to visualise vascular uptake [12]. As a refinement of this technique, time-resolved 3D MR angiography techniques can be used to detect vascular uptake through monitoring of a test injection of gadolinium-enhanced sterile saline. The safety of gadolinium-based contrast agents in combination with steroids has been shown in lumbar spinal injection procedures [45]. Discography has a minimal rate of discitis of about 0.17 % per patient using the two-needle co-axial technique and prophylactic antibiotics [46]. Instead of the single needle technique used in this initial evaluation, a two-needle co-axial technique can be used.

**Fig. 6** MR-guided discography using image overlay navigation. **a** Planning of the virtual needle path (grey arrow) into the nucleus pulposus of the L4–L5 disk (white arrow) using the Perk Station. **b** Axial turbo spine echo MR image following needle placement demonstrates the tip of the needle (grey arrows) in the nucleus pulposus of the disk (white arrow). The black arrow indicates the spared L4 nerve root. **c** Sagittal, T1-weighted MR image with spectral fat saturation following discography L1–L5 shows the injected material (white arrows) outlining the nucleus pulposus L1–L4. Note the obliquity of the L5–S1 disk (grey arrow), which did not allow for puncture using an axial needle path
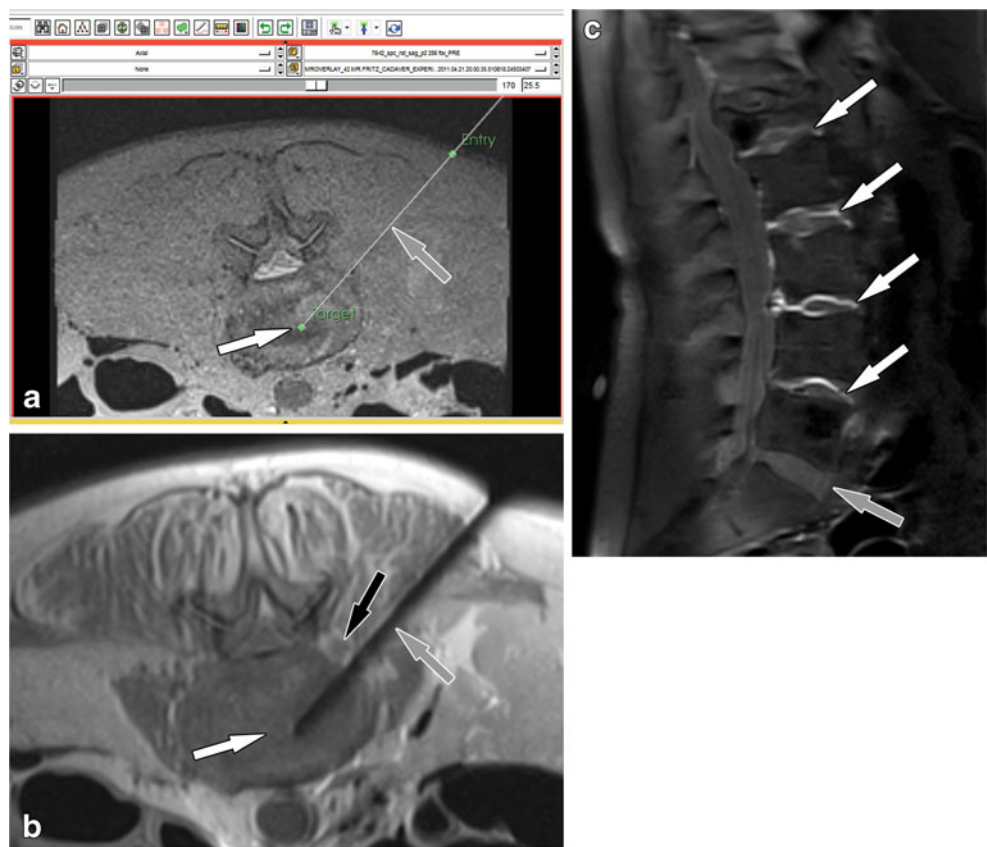


In its current version, MRI guidance with the IOS is limited to only axial plane needle paths. An axial needle trajectory was adequate to access most of the targets; however, none of the significantly more oblique L5-S1 disks was accessible (Fig. 6). In order to enable access to such targets, we plan to include a tilting function in the IOS.

Our study design had limitations. Although efforts were made to use a high number of cadavers, multiple procedures were performed in one cadaver, which may result in clustering effects. Owing to the use of cadavers, effects of patient motion and respiration were not apparent in our study, which may influence the performance of static image overlay navigation.

Based on the performance of the IOS of spinal injection procedures in this cadaver trial, we plan to extend our work to a clinical trial, which will yield additional data about logistics, time requirements, patient acceptance and cost.

In summary, we conclude that MR-guided lumbar spinal injection procedures with use of image overlay navigation resulted in a high success rate. With use of augmented reality MRI guidance, no inadvertent puncture of vulnerable, non-targeted anatomical structures occurred.

**Table 2** Needle adjustments

| Procedures | Needle adjustment | | Trajectory change | | Advancement | | Withdrawal | |
|---|---|---|---|---|---|---|---|---|
| | *n* | % of total | *n* | % of total | *n* | % of total | *n* | % of total |
| Epidural injection | 1 | 0.6 | 0 | 0.0 | 1 | 0.6 | 0 | 0.0 |
| Selective spinal nerve root injection | 21 | 11.9 | 5 | 2.8 | 10 | 5.7 | 6 | 3.4 |
| Facet joint injection | 10 | 5.7 | 8 | 4.5 | 2 | 1.1 | 1 | 0.6 |
| Medial branch nerve block | 0 | 0.0 | 0 | 0.0 | 0 | 0.0 | 0 | 0.0 |
| Discography | 15 | 8.5 | 11 | 6.3 | 2 | 1.1 | 2 | 1.1 |
| Total | 47/176 | 26.7 | 24/176 | 13.6 | 15/176 | 8.5 | 9/176 | 5.1 |

% of total is given relative to 176 targets

**Table 3** Procedure times

| Procedure | Median [min] | Min [min] | Max [min] |
|---|---|---|---|
| Epidural injection | 8.6 | 6 | 16 |
| Selective spinal nerve root injection | 10.0 | 6 | 18 |
| Facet joint injection | 10.2 | 6 | 19 |
| Medial branch nerve block | 10.0 | 5 | 19 |
| Discography | 10.0 | 5 | 17 |

# References

1. Fritz J, Niemeyer T, Clasen S et al (2007) Management of chronic low back pain: rationales, principles, and targets of imaging-guided spinal injections. Radiographics 27:1751–1771

2. Carrino JA, Morrison WB, Parker L, Schweitzer ME, Levin DC, Sunshine JH (2002) Spinal injection procedures: volume, provider distribution, and reimbursement in the US Medicare population from 1993 to 1999. Radiology 225:723–729

3. Krombach GA, Schmitz-Rode T, Wein BB et al (2000) Potential of a new laser target system for percutaneous CT-guided nerve blocks: technical note. Neuroradiology 42:838–841

4. Nawfel RD, Judy PF, Silverman SG, Hooton S, Tuncali K, Adams DF (2000) Patient and personnel exposure during CT fluoroscopy-guided interventional procedures. Radiology 216:180–184

5. Paulson EK, Sheafor DH, Enterline DS, McAdams HP, Yoshizumi TT (2001) CT fluoroscopy–guided interventional procedures: techniques and radiation dose to radiologists. Radiology 220:161–167

6. Wagner AL (2004) Selective lumbar nerve root blocks with CT fluoroscopic guidance: technique, results, procedure time, and radiation dose. AJNR Am J Neuroradiol 25:1592–1594

7. Wagner LK (2000) CT fluoroscopy: another advancement with additional challenges in radiation management. Radiology 216:9–10

8. Blanco SR, Carrino JA (2005) Musculoskeletal interventional MR imaging. Magn Reson Imaging Clin N Am 13:519–532

9. Fritz J, Henes JC, Thomas C et al (2008) Diagnostic and interventional MRI of the sacroiliac joints using a 1.5-T open-bore magnet: a one-stop-shopping approach. AJR Am J Roentgenol 191:1717–1724

10. Fritz J, Clasen S, Boss A et al (2008) Real-time MR fluoroscopy-navigated lumbar facet joint injections: feasibility and technical properties. Eur Radiol 18:1513–1518

11. Fritz J, Thomas C, Tzaribachev N et al (2009) MRI-guided injection procedures of the temporomandibular joints in children and adults: technique, accuracy, and safety. AJR Am J Roentgenol 193:1148–1154

12. Fritz J, Thomas C, Clasen S, Claussen CD, Lewin JS, Pereira PL (2009) Freehand real-time MRI-guided lumbar spinal injection procedures at 1.5 T: feasibility, accuracy, and safety. AJR Am J Roentgenol 192:W161–W167

13. Fritz J, Tzaribachev N, Thomas C et al (2010) Evaluation of MR imaging guided steroid injection of the sacroiliac joints for the treatment of children with refractory enthesitis-related arthritis. Eur Radiol 21:1050–1057

14. Ojala R, Vahala E, Karppinen J et al (2000) Nerve root infiltration of the first sacral root with MRI guidance. J Magn Reson Imaging 12:556–561

15. Ojala R, Klemola R, Karppinen J, Sequeiros RB, Tervonen O (2001) Sacro-iliac joint arthrography in low back pain: feasibility of MRI guidance. Eur J Radiol 40:236–239

16. Smith KA, Carrino J (2008) MRI-guided interventions of the musculoskeletal system. J Magn Reson Imaging 27:339–346

17. Hushek SG, Martin AJ, Steckner M, Bosak E, Debbins J, Kucharzyk W (2008) MR systems for MRI-guided interventions. J Magn Reson Imaging 27:253–266

18. Lewin JS, Petersilge CA, Hatem SF et al (1998) Interactive MR imaging-guided biopsy and aspiration with a modified clinical C-arm system. AJR Am J Roentgenol 170:1593–1601

19. Weiss CR, Nour SG, Lewin JS (2008) MR-guided biopsy: a review of current techniques and applications. J Magn Reson Imaging 27:311–325

20. Weiss CR, Marker DR, Fischer GS, Fichtinger G, Machado AJ, Carrino JA (2011) Augmented reality visualization using image-overlay for MR-guided interventions: system description, feasibility, and initial evaluation in a spine phantom. AJR Am J Roentgenol 196:W305–W307

21. Fischer GS, Deguet A, Schlattman D et al (2006) MRI image overlay: applications to arthrography needle insertion. Stud Health Technol Inform 119:150–155

22. Fichtinger G, Deguet A, Masamune K et al (2005) Image overlay guidance for needle insertion in CT scanner. IEEE Trans Biomed Eng 52:1415–1424

23. Fritz J, U-Thainual P, Ungi T et al (2011) Augmented reality visualization using image-overlay for MR-guided interventions: accuracy for lumbar spinal procedures with a 1.5-Tesla MRI scanner. AJR Am J Roentgenol 198:W266–W273

24. Vikal S, Thainual P, Carrino JA, Iordachita I, Fischer GS, Fichtinger G (2010) Perk Station–Percutaneous surgery training and performance measurement platform. Comput Med Imaging Graph 34:19–32

25. Gering DT, Nabavi A, Kikinis R et al (2001) An integrated visualization system for surgical planning and guidance using image fusion and an open MR. J Magn Reson Imaging 13:967–975

26. Obesity: preventing and managing the global epidemic. Report of a WHO consultation (2000) World Health Organ Tech Rep Ser 894: i–253

27. Carrino JA, Lurie JD, Tosteson AN et al (2009) Lumbar spine: reliability of MR imaging findings. Radiology 250:161–170

28. Streitparth F, Walter T, Wonneberger U et al (2010) Image-guided spinal injection procedures in open high-field MRI with vertical field orientation: feasibility and technical features. Eur Radiol 20:395–403

29. Sequeiros RB, Ojala RO, Klemola R, Vaara TJ, Jyrkinen L, Tervonen OA (2002) MRI-guided periradicular nerve root infiltration therapy in low-field (0.23-T) MRI system using optical instrument tracking. Eur Radiol 12:1331–1337

30. Sequeiros RB, Klemola R, Ojala R, Jyrkinen L, Vaara T, Tervonen O (2003) Percutaneous MR-guided discography in a low-field system using optical instrument tracking: a feasibility study. J Magn Reson Imaging 17:214–219

31. Streitparth F, Hartwig, Schnackenburg B et al (2011) MR-guided discography using an open 1 Tesla MRI system. Eur Radiol 21:1043–1049

32. Fritz J, Pereira PL (2007) MR-Guided pain therapy: principles and clinical applications. Rofo 179:914–924

33. Moche M, Trampel R, Kahn T, Busse H (2008) Navigation concepts for MR image-guided interventions. J Magn Reson Imaging 27:276–291

34. Sullivan WJ, Willick SE, Chira-Adisai W et al (2000) Incidence of intravascular uptake in lumbar spinal injection procedures. Spine (Phila Pa 1976) 25:481–486

35. Furman MB, O'Brien EM, Zgleszewski TM (2000) Incidence of intravascular penetration in transforaminal lumbosacral epidural steroid injections. Spine (Phila Pa 1976) 25:2628–2632

36. Manchikanti L, Cash KA, Pampati V, Damron KS, McManus CD (2004) Evaluation of lumbar transforaminal epidural injections with needle placement and contrast flow patterns: a prospective, descriptive report. Pain Physician 7:217–223

37. Goodman BS, Lincoln CE, Deshpande KK, Poczatek RB, Lander PH, Devivo MJ (2005) Incidence of intravascular uptake during fluoroscopically guided lumbar disc injections: a prospective observational study. Pain Physician 8:263–266

38. Lee CJ, Kim YC, Shin JH et al (2008) Intravascular injection in lumbar medial branch block: a prospective evaluation of 1433 injections. Anesth Analg 106:1274–1278, table

39. Kennedy DJ, Dreyfuss P, Aprill CN, Bogduk N (2009) Paraplegia following image-guided transforaminal lumbar spine epidural steroid injection: two case reports. Pain Med 10:1389–1394

40. Lyders EM, Morris PP (2009) A case of spinal cord infarction following lumbar transforaminal epidural steroid injection: MR imaging and angiographic findings. AJNR Am J Neuroradiol 30:1691–1693

41. Glaser SE, Falco F (2005) Paraplegia following a thoracolumbar transforaminal epidural steroid injection. Pain Physician 8:309–314

42. Houten JK, Errico TJ (2002) Paraplegia after lumbosacral nerve root block: report of three cases. Spine J 2:70–75

43. Thefenne L, Dubecq C, Zing E et al (2010) A rare case of paraplegia complicating a lumbar epidural infiltration. Ann Phys Rehabil Med 53:575–583

44. Lenoir T, Deloin X, Dauzac C, Rillardon L, Guigui P (2008) Paraplegia after interlaminar epidural steroid injection: a case report. Rev Chir Orthop Reparatrice Appar Mot 94:697–701

45. Shetty SK, Nelson EN, Lawrimore TM, Palmer WE (2007) Use of gadolinium chelate to confirm epidural needle placement in patients with an iodinated contrast reaction. Skeletal Radiol 36:301–307

46. Sharma SK, Jones JO, Zeballos PP, Irwin SA, Martin TW (2009) The prevention of discitis during discography. Spine J 9:936–943